## Title

Forced Vibration Testing of a Four-Story Reinforced Concrete Building Utilizing the nees@UCLA Mobile Field Laboratory



## Journal

Center for Embedded Network Sensing, 24(4)

## Authors

Yu, Eunjong
Skolnik, Derek
Whang, Daniel H.
et al.

## Publication Date

2008-11-01

## DOI

10.1193/1.2991300

Peer reviewed

# Forced Vibration Testing of a Four-Story Reinforced Concrete Building Utilizing the *nees*@UCLA Mobile Field Laboratory

**Eunjong Yu,[a] Derek Skolnik,[b] Daniel H. Whang,[c] M.EERI, and John W. Wallace,[b] M.EERI**

The *nees*@UCLA mobile field laboratory was utilized to collect forced and ambient vibration data from a four-story reinforced concrete (RC) building damaged in the 1994 Northridge earthquake. Both low amplitude broadband and moderate amplitude harmonic excitation were applied using a linear shaker and two eccentric mass shakers, respectively. Floor accelerations, interstory displacements, and column and slab curvature distributions were monitored during the tests using accelerometers, linear variable differential transformers (LVDTs) and concrete strain gauges. The use of dense instrumentation enabled verification of common modeling assumptions related to rigid diaphragms and soil-structure-interaction. The first six or seven natural frequencies, mode shapes, and damping ratios were identified. Significant decreases in frequency corresponded to increases in shaking amplitude, most notably in the N-S direction of the building, most likely due to preexisting diagonal joint cracks that formed during the Northridge earthquake. [DOI: 10.1193/1.2991300]

## INTRODUCTION

Field testing of full-scale structures using mechanical shakers plays an important role in determining the dynamic properties of structures to enable improved modeling of structural systems subjected to combined gravity and lateral loads. Given this, a large number of studies have been conducted using ambient and low-level forced vibrations (well within the linear range, unlikely to produce significant concrete cracking) to capture the responses of buildings (e.g., Hudson 1960, 1961, 1962; Jennings et al. 1972; Stephen and Bouwkamp 1977; Hudson 1977; Galambos and Mayes 1979), dams (e.g., Petrovski et al. 1974; Bolt and Hudson 1975; Abdel-Ghaffar and Scott 1980), foundation systems (e.g., Muto and Kobayashi 1973; Foutch and Jennings 1978; Imamura et al. 1996), bridges (e.g., Dye and Halling 2002), and nuclear power plants (e.g., Ibáñez et al. 1981). These studies resulted in substantial advances in field testing capabilities. However, due to the technological limits that naturally existed at the time of these tests, most

[a] Hanyang University, Dept of Architectural Engineering, 17 Haendang-dong, Seongdong-gu, Seoul, Korea
[b] University of California, Dept. of Civil & Envir. Engrg., 5731 Boelter Hall, Los Angeles, CA 90095-1593
[c] Engineer, Exponent 320 Goddard, Irvine, CA 92618


*Earthquake Spectra,* Volume 24, No. 4, pages 969–995, November 2008; 

were conducted at relatively low-level, harmonic excitation with a relatively small number of sensors. A primary goal of this research is to build upon prior research accomplishments by incorporating state-of-the-art data acquisition and sensor technologies and to provide detailed archival documentation and data that are of value and interest to both researchers and practicing engineers.

High quality field performance data offer valuable information against which analysis procedures, code provisions, and other tests results are supported. However, several factors have limited advances in field testing in recent years, including (1) the inability of artificial (forced) vibration sources to impart moderate-to-large amplitude vibrations on test structures (e.g., likely to produce concrete cracking, approaching component yield), (2) the inability of traditional vibration sources to excite structures with broadband inputs to better represent realistic seismic motions, and (3) practical difficulties associated with deploying a sufficiently large sensor array to assess detailed component behavior. Permanent instrumentation of structures, such as provided by the California Strong Motion Instrumentation Program (CSMIP 2006), addresses some of these needs and also provides important information on the distribution of responses over large geographic areas; however, relatively few sensors typically consisting exclusively of accelerometers are deployed at a limited number of floors (typically 10 to 15 sensors). Although a few permanently instrumented structures are embedded with relatively dense and high quality accelerometer networks, like the UCLA Factor Building (Skolnik et al. 2006), an earthquake capable of producing at least moderate-amplitude responses is desirable to generate data of interest.

The University of California, Los Angeles NEES Equipment Site (*nees*@UCLA) was established by the National Science Foundation George E. Brown Jr. Network for Earthquake Engineering Simulation (NEES) to address these limitations. The *nees*@UCLA equipment portfolio includes (1) large capacity eccentric mass shakers for harmonic excitation, (2) a linear mass shaker for broadband seismic simulation at low force levels, (3) sensors for monitoring acceleration and/or displacement responses, (4) wireless field ADC data loggers with time synchronization capabilities that efficiently transfer data from the test structure to the high performance mobile network, and (5) a high performance mobile network that receives and locally stores data at a mobile command center deployed near the test site, transmits and broadcasts selected data via satellite for teleobservation of experiments (Whang et al. 2004).

The advanced field testing capabilities of the *nees*@UCLA Site were deployed on a four-story reinforced concrete building in Sherman Oaks, California during the summer of 2004. The building suffered significant damage in the 1994 Northridge earthquake and was eventually demolished in the summer of 2007. Previous studies (Sabol 1994; Aschheim and Moehle 1995; Hueste and Wight 1997) documented some of the building damage and reported results of analytical studies to assess reasons for the observed damage. The results of these studies were inconclusive, in part due to the considerable uncertainty in modeling the structural system. Consequently, ambient and forced vibration testing was performed to collect field measurement data that could be used to evaluate the validity of prior analytical models as well as to provide essential data for model calibration. Furthermore, test data of full-scale structures with significant levels of shaking

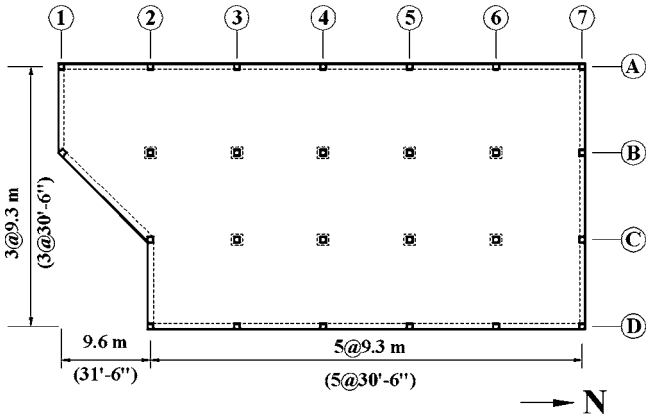


**Figure 1.** Typical floor plan of Four Seasons office building.

and high-density spatial resolution of instrumentation are rare or not widely available and publicly archived. Therefore, another objective of this study was to generate a truly unique and detailed dataset in terms of high-density spatial resolution that will be archived in the NEES data repository (http://www.nees.org). This dataset could be useful for earthquake engineering researchers to improve understanding of the dynamic response of real buildings, and for damage detection studies.

In the sections that follow, we document the building condition, provide an overview of the *nees@*UCLA equipment, describe the testing and instrumentation plan, and finally provide results obtained using the test data. In addition to the study described herein, several parallel collaborative "payload" projects were conducted by researchers at UC Irvine on the use of visualization to monitor non-structural elements and science laboratory equipment (Nastase 2005), and researchers at USC on the use of novel MEMS/wireless sensor arrays (Paek et al. 2005). These studies are beyond the scope of this paper.

## BUILDING AND DAMAGE SURVEY

### GENERAL DESCRIPTION

The four story reinforced concrete office building, referred to as the Four Seasons Building is located in Sherman Oaks, California and was constructed in 1977. The structural system consists of a perimeter beam-column frame and an interior post-tensioned slab-column gravity frame with drop panels. Figure 1 shows a plan view of the building. Typical interior gravity frames consist of a 8.5 in. deep post-tensioned flat slab constructed of 4000 psi lightweight concrete and 24 in. square columns with 48 in. square 7.5 in. deep drop panels of 5000 psi normal weight concrete. The roof consists of a lightweight concrete post-tensioned flat slab that varies in thickness from 7.5 to 13 in. to provide the required gradient for adequate drainage. Reinforcement with specified yield strength of 60,000 psi was used for longitudinal and transverse reinforcement in all ma-

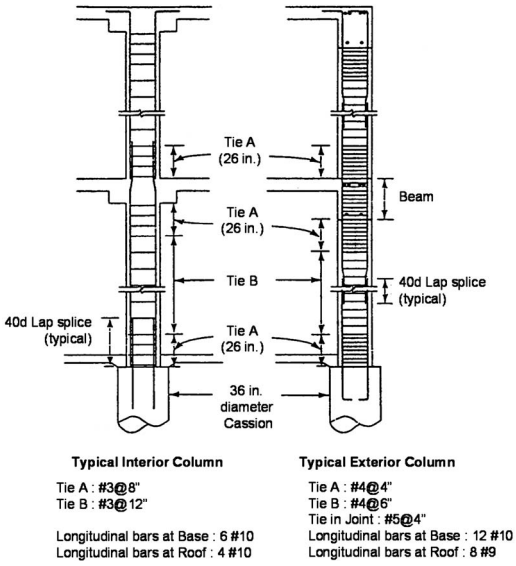


**Figure 2.** Typical (a) interior column and (b) exterior column reinforcement.

jor structural members. Seven wire post-tensioning strands having a minimum ultimate tensile strength of 270,000 psi were used for the unbonded post-tensioned slab. Typical interior columns of the slab-column frame are reinforced with either 4 or 6 #10 longitudinal reinforcing bars enclosed in #3 hoops spaced at 8 to 12 in. (Figure 2).

Lateral seismic resistance is provided by a perimeter frame composed of 24 in. square columns constructed of 5000 psi normal-weight concrete and beams of 4000 psi lightweight concrete. The perimeter beams are 24 in. wide by 30 in. deep, except for beams on the second floor level which are 24 in. wide by 36 in. deep. Typical beams are reinforced with two #10 top bars and three to four #11 bottom bars, and typical perimeter columns are reinforced with 8 #9 to 12 #10 bars with #4 hoops at 4 to 6 in. on center. Transverse reinforcement was provided within the critical regions of the beams and columns to satisfy detailing requirements for a Special Moment Resisting Space Frame (SMRSF) per UBC-76 (ICBO 1976). The foundation system consists of bell caissons with a shaft diameter of 36 in. and bell diameters of either 5.5 ft, 7.5 ft, or 8.5 ft. The caissons are connected by normal weight concrete (3000 psi) grade beams. Additional details and detailed drawings of the structural and foundation system, connection details and material properties are provided in Yu (2005).

No ground motions were recorded at the site during the earthquake; however, a record was obtained in the basement of a 13-story RC building (CSMIP station No. 24322) approximately 0.3 miles south of the site. Figure 3 displays the response spectra derived from the NS component. Recorded horizontal peak ground accelerations in the basement of the nearby building were 0.45 g and 0.23 g in the north-south and east-west directions, respectively. Although the ground motions at the test building may vary from

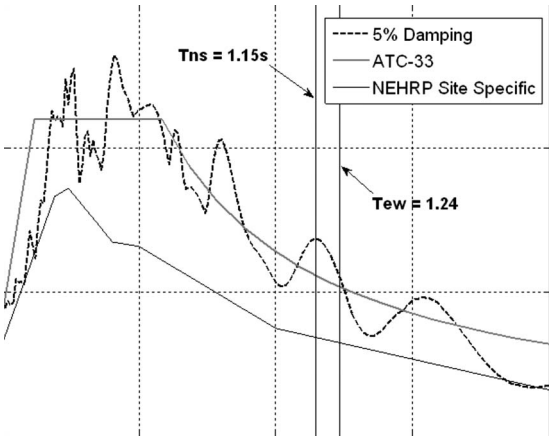


**Figure 3.** Response spectra obtained from N-S component of recorded acceleration during Northridge at basement floor of nearby 13-story building (CSMIP 24322). Also included are the site specific spectra provided by NEHRP as reported in Aschheim and Moehle (1995) and the derived ATC-33 spectrum. Finally, the fundamental NS and EW periods identified during EMS shaking are marked.

those recorded at the nearby building, the recorded peak accelerations indicate that relatively strong shaking occurred nearby the test structure. Additionally, site specific motions (also shown in Figure 3) for the test building were derived as part of the Building Seismic Safety Council funded case studies for the 50% draft of ATC-33 (Aschheim and Moehle 1995) and also indicate that strong shaking occurred at the test building site.

## DETAILED SURVEY OF PREEXISTING DAMAGE

Detailed visual inspections of the building were performed prior to forced-vibration testing to document the existing structural condition. Particularly severe damage was observed at slab-column connections due to slab punching shear failure around the perimeter of the drop panels. The most dramatic failures were observed at the south end of the second floor level (column B2) and the north end of the third floor level (column B6, Figure 4a).

Diagonal cracks were observed within the beam-column joint regions (Figure 4b) along the east and west perimeter frames, primarily at the third floor level between columns A4 to A6 and columns D4 to D6. Minor concrete cover spalling was observed were the cracks crossed at the middle of some joints, and the diagonal cracks often extended up to the floor slab. No joint cracks were noted in the north and south perimeter frames except for column C7 at the roof level. The damage survey also indicated that a majority of the perimeter girders in both directions had minor to moderate concrete crushing at the joint interface, and most of the perimeter columns had flexural cracks


**Figure 4.** Earthquake damage to the building: (a) punching shear failure (Column B6 at the third floor level), and (b) diagonal crack on beam-column joint (Column A4 at the third floor level) (c) & (d) detachment of partition and infill wall from column (Column A1 at the first floor level).

distributed over the height on all four column faces. Overall, the perimeter frame damage patterns indicate that the building experienced considerably more deformations in the N-S direction than the E-W direction.

Partition walls (metal studs and wallboard) and masonry walls at the ground floor were detached and separated from adjacent structural members Figure 4c and 4d, indicating that the building experienced substantial lateral deformations during the earthquake. These observations indicate that non-structural partitions were unlikely to contribute to the lateral strength and stiffness of the building during the subsequent forced vibration tests conducted as part of this study.

## PREVIOUS STUDIES

Several studies were conducted to document the building damage (Sabol 1994) and to assess reasons for the damage (Aschheim and Moehle 1995; Hueste and Wight 1997). Aschheim and Moehle performed linear and nonlinear static pushover analyses using the 50% draft of ATC-33. To model slab-column punching failures, a linear model relating rotation capacity ($\theta_{\max}$) and gravity shear to nominal shear strength ratio ($V_g/V_0$) was defined using the following points: $(V_g/V_0, \theta_{\max})=(1.00, 0)$ and (0, 0.04). Results obtained from their analyses were not consistent with the degree and distribution of the observed damage. The nonlinear analyses indicated that perimeter frame column hinging and yielding of slab reinforcement at slab-column connections; however, the slab-column connection rotations were below the estimated rotation capacity from the assumed rotation-shear strength ratio punching model. They hypothesized that torsional response might have increased connection rotation demands based on the observation that punching failures were more severe at the south end of the building. Aschheim and Moehle amplified rotation demands from the nonlinear pushover analysis by a factor of two to account for torsion; however, the computed rotation demands for the given site-specific demand spectrum were still only about one-half of those expected to produce a punching failure. They cited five possible reasons for this discrepancy: (1) ground motions at the site were more severe than those used; (2) properties of the analytical model

differed significantly from those of the actual building; (3) torsional response of the building was more significant then assumed; (4) vertical response was significant; and (5) the tentative model used to assess slab-column punching was not conservative. As well, they did not consider the impact of joint damage on the flexibility of the structural system.

Hueste and Wight (1997) performed both nonlinear static pushover and nonlinear dynamic analyses using ground motions recorded in the basement of the nearby 13-story building (CSMIP station No. 24322). Analysis results based on the design drawings did not indicate punching problems at the slab-column connections. However, inspection of one of the damaged connections revealed that reinforcement had not been placed as indicated on the drawings, which reduced the effective slab depth and resulted in greater potential for slab-column punching failures. Subsequent static and dynamic analysis results using revised punching capacities reduced to represent as-built conditions indicated potential for punching failures at all first and second floor slab-column connections. Parametric studies showed that building drift and slab-column punching were relatively insensitive to the assumed value used in the analyses for rebar yield stress, and that foundation flexibility and vertical ground motions did not significantly affect the dynamic response or the punching shear stresses.

In summary, although prior analytical studies indicated some potential for damage at the slab column connections, the degree and distribution of the observed damage were substantially greater than could be predicted using the analytical tools available. Damage was concentrated at the interior slab-column connections with relatively little damage to the perimeter moment frame, consisting of minor cracking and concrete spalling. Given the condition of the perimeter frame, significant residual lateral displacements were unlikely. Conducting forced-vibration tests on the building provided a unique opportunity to collect data that could be used to improve and update models for moderate-level responses to enable more detailed follow-up studies to assess reasons for the building damage in the Northridge earthquake. The material that follows documents the tests conducted and preliminary findings, and also provides the basis for more detailed follow-up studies.

## *NEES*@UCLA EQUIPMENT OVERVIEW

Equipment, instrumentation, and data acquisition systems integrated into the Network for Earthquake Engineering Simulation (NEES) mobile field laboratory at UCLA (*nees*@UCLA) were deployed for forced-vibration testing. An overview of the *nees*@UCLA portfolio is provided in the following subsections. Although the equipment used for this study is not unique, a comprehensive description is provided to inform readers of the current available commercial-off-the-shelf systems, since the *nees*@UCLA facility is shared-use facility that encourages outside users. More detailed information is provided by Whang et al. (2004), Yu (2005), and on the *nees*@UCLA website (http://nees.ucla.edu).

(a) (b)

**Figure 5.** Field shakers: (a) eccentric mass shaker (EMS) and (b) linear mass shaker (LMS).

## FIELD SHAKERS

Two, large capacity, eccentric mass shakers (EMS) (ANCO Model MK-15) and a modest-capacity linear mass shaker (LMS) were anchored to the roof of the building as vibration sources (Figure 5). A single MK-15 shaker develops unidirectional harmonic forces with a peak force output of 100 kips with two counter-rotating baskets. The force generated by each EMS, $P$, is expressed as:

$$P(t) = 2m_e\omega^2 \sin(\omega t) \tag{1}$$

where $m_e$ is the mass-eccentricity constant that depends on the magnitude and distribution of masses used in the baskets, and $\omega$ is the circular frequency of rotation in radian/sec. In the present tests, two different basket configurations were used as shown in Table 1. The limiting frequency associated with the peak force depends on the magnitude and distribution of steel bricks used in the baskets.

The two MK-15 shakers can be synchronized at variable phase angles using a closed loop control system with pulse marker signal feedback. The EMS were positioned at the north and south ends of the roof to maximize the torsional excitation that could be produced, while also enabling translational excitation in the N-S and E-W directions, as shown in Figure 6.

The LMS system can generate broadband excitations at low force levels to enable efficient assessment of modal properties. The LMS is driven by a hydraulic actuation system capable of moving a nominal weight of 5 kips with a peak force of 15 kips through a stroke of ±15 inch. The LMS was mounted at a 45° angle form the perimeter

**Table 1.** Mass-eccentricity of each basket and limiting frequencies

| | Empty basket | Half-full basket |
|---|---|---|
| Mass-eccentricity | 16786 lb-in | 56620 lb-in |
| Limiting frequency[a] | 5.40 Hz | 2.95 Hz |

[a] The frequency at which the shaker achieves the maximum force amplitude for that mass-eccentricity

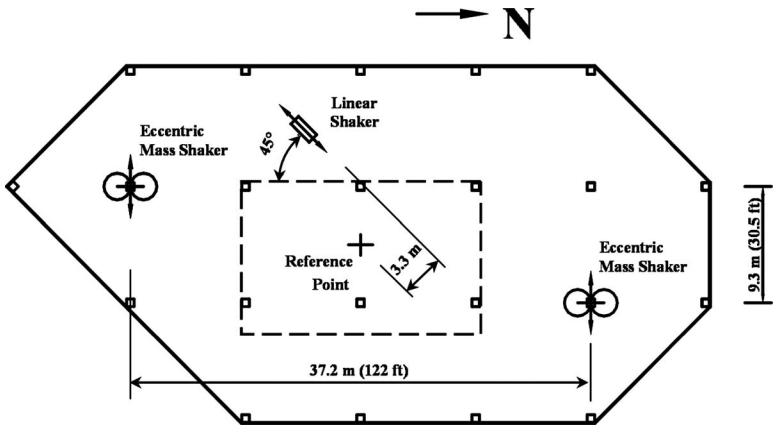


**Figure 6.** Shaker locations.

frames about 11 ft away from the approximate center of the roof (the reference point) as shown in Figure 6. This location and orientation were selected to impart approximately equivalent levels of excitation in N-S and E-W translations while also providing torsional excitation.

## INSTRUMENTATION AND DATA ACQUISITION

A dense array of sensors was deployed within the building prior to the tests. A total of 16 triaxial and 27 uniaxial force-balance accelerometers (Kinemetrics Episensor ES-T and ES-U, respectively) were mounted on floor slabs, 26 linear variable displacement transducers (Trans-Tek, Series 240 DC LVDT) were mounted on beams and on columns, and 96 strain gauges (TML, PL-60-11-5L) were affixed to slab and column surfaces to allow determination of accelerations, interstory drift, as well as slab and column curvature distributions. Figure 7 shows the approximate locations of the sensors distributed throughout the building. Therefore, a total of 197 data channels were used to measure

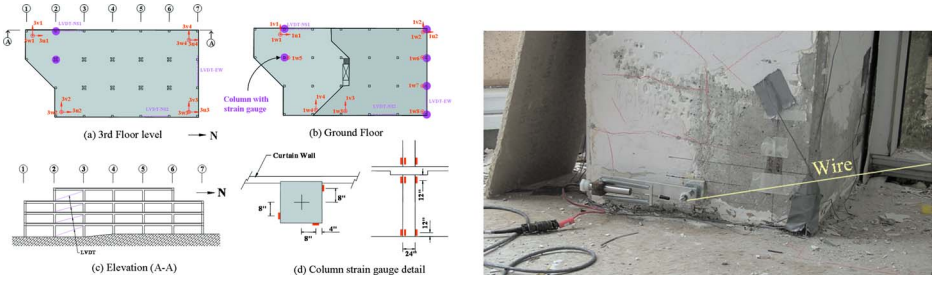


**Figure 7.** Instrumentation plan of (a) third floor (typical), (b) Ground floor, (c) West elevation, (d) location of column strain gauge, and (e) LVDT set up.

the building responses imparted by either the LMS or the EMS. In addition, five channels of data were collected for tests utilizing the EMS (four pulse markers) and an accelerometer on the moving mass for the LMS tests to enable determination of the applied forcing functions.

Ignoring vertical movements, three channels of horizontal acceleration (two channels aligned to one direction and the third channel perpendicular to the first two sensors) are needed to describe the lateral movement of a floor if the floor is assumed to be rigid in plane (i.e., rigid diaphragm assumption). Given the thickness of the post-tensioned floor (8.5 in.) and roof slab (7.5 to 13 in.), respectively, for the building, the floor diaphragm of the building was assumed to be rigid. In this study, four triaxial accelerometers were mounted at approximately the four corners of the building to provide additional data and to protect against data loss in the case of instrument failure and/or data (packet) loss during wireless data acquisition. Furthermore, additional accelerometers were installed on the ground floor to measure potential rocking and translation of the ground floor. Interstory displacements were measured using 12 LVDTs mounted between columns A2-A3, D5-D6 and B7-C7 from the ground floor to the roof between every floor, as shown in Figure 7c. The LVDTs were mounted using a spring loaded mount to pretension a wire that extended from the sensor at the bottom of a column at the floor level to the top of a column at the ceiling level, Figure 7e. The spring stiffness was selected to minimize the interaction between the vibrating sensor and the vibrating building, based on preliminary testing.

To derive column curvature distributions from the ground floor to the roof, 48 concrete strain gauges were attached on three column faces just above and below the floor slab at each story along columns A2 and B2. A total of 34 concrete strain gauges also were affixed to the top and bottom slab surfaces adjacent to the column at the third and fourth floor slabs to enable calculation of slab curvature distributions. Slab and column strains for connections with and without visible damage were monitored to determine the residual moment transfer capacity of damaged connections, i.e., if moment and shear transfer at connections was consistent with the degree of observed (visual) damage.

Data acquisition was performed using two separate systems, one for the accelerometers and LVDTs and the other for the concrete strain gauges. Data from both systems were GPS time-stamped to ensure synchronization. Figure 8 shows a schematic of the data acquisition system for accelerometers and LVDTs. These sensors were connected to 19 units of 24-bit, 6-channel Kinemetrics Q330 dataloggers, where analog signals were digitized, time-stamped and stored to a local memory buffer as data packets. The data packets were transmitted using 802.11b wireless networking technology to a Data Concentrator (DC) located on the roof floor via four Wireless Access Point (WAP) modules distributed throughout the building. The DC houses a UNIX workstation running Antelope (data acquisition software for Kinemetrics system) and wireless networking equipment. The DC consolidates and broadcasts collected data and video streams wirelessly to the mobile command center (MCC) which is a truck with integrated mobile computing facilities and satellite communication systems. The data transfer from the DC to the MCC located near the test building ($\sim$300 ft) was accomplished via standard 802.11b

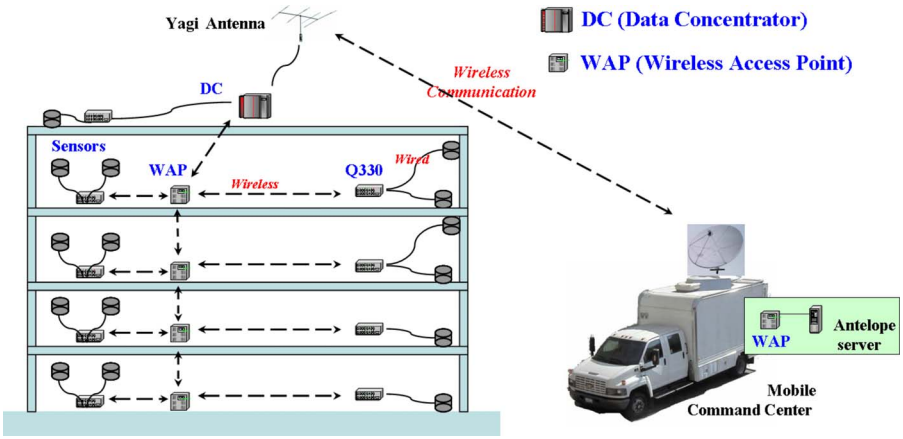


**Figure 8.** A schematic drawing of Kinemetrics DAQ system.

wireless and TCP/IP networking protocols, using a Yagi (unidirectional, high-gain antenna) at the penthouse roof and a parabola antenna attached to the MCC.

The concrete strain gauges were hardwired to three separate data acquisition systems consisting of National Instrument (NI) boards and a computer running Labview Version 7.0 (National Instruments 2003). Each of these systems is equipped with a 32-channel signal conditioning module, a GPS receiver and a high resolution counter-timer board to enable data time synchronization. All three of the 32-channel systems were located on the south end of the second floor due to security reasons, thereby requiring long lead wires for the gauges. Resistance of lead wires for each channel were measured and compensated for during data processing.

## TESTING PROGRAM

The testing consisted of a series of forced vibration tests using the LMS and EMS, respectively, and ambient vibration tests, as shown in Table 2. The LMS was used to generate broadband excitations to assess modal properties of the building using system identification techniques. During the moderate-amplitude sinusoidal vibrations obtained by synchronized operation of the two large-capacity EMS, interstory displacement, slab curvature, and column curvature distributions were investigated. Before and after forced vibration testing, ambient vibrations were measured to investigate potential drift of modal properties.

The test sequence is shown in Table 2. After completing the first series of forced vibration tests, additional structural damage was induced to the perimeter frame by cutting top reinforcement at five locations along Line A of the third floor (Yu 2005). Vibration measurements were subsequently obtained using the LMS and the EMS, and from ambient vibrations, to investigate potential changes in responses due to the induced damage. The induced damage did not noticeably influence the natural frequencies, as

**Table 2.** Test sequence

| Date[a] | Test |
|---|---|
| 07/02/04 | Ambient vibration measurement—Run1 |
| 06/22/04 to 07/13/04 | E-W translational/Torsional excitation with *empty* baskets |
| 07/14/04 to 07/19/04 | E-W translational/Torsional excitation with *half-full* baskets |
| 07/19/04 | Ambient vibration measurement—Run2 |
| 07/19/04 | Linear shaker test—Run1 |
| 07/22/04 | N-S translational excitation with *half-full* baskets |
| 07/28/04 | N-S translational excitation with *empty* baskets |
| 07/30/04 | Impose additional structural damage by beam end cutting |
| 08/02/04 | N-S translational excitation with *empty* baskets |
| 08/02/04 | Linear shaker test—Run2 |
| 08/03/04 | E-W translational/Torsional excitation with *empty* baskets |
| 08/03/04 | Ambient vibration measurement—Run3 |

[a] month/date/year

results obtained before and after the damage was induced were essentially the same. The authors believe that the induced damage was too "localized" to be detected by changes in global parameters (Doebling et al. 1996); however, these data are mentioned here only as they could be potentially useful for future studies since the data will be archived and broadly available to the community.

## LINEAR SHAKER AND AMBIENT VIBRATION TESTS

A white noise-type broadband excitation, obtained by band pass filtering (fifth-order Butterworth filter) random numbers to cut out the frequency content below 0.5 Hz and above 10 Hz, was applied to the building using the LMS at the roof of the building. The acceleration of the moving mass of the LMS was measured by a uniaxial accelerometer to determine the history of the input force.

Raw acceleration data were detrended to compensate for temperature drift, and then decimated from 100 to 50 samples per second (sps) to enable more efficient data analysis. The MATLAB (MathWorks, Inc. 2004) command, *resample*, which applies an anti-aliasing filter to the data during the resampling process, was used. From the decimated records, three components of story acceleration, based on a rigid floor diaphragm assumption, were calculated as follows:

$$\theta_c = -\frac{u_i - u_j}{y_i - y_j} \quad \text{or} \quad \theta_c = \frac{v_i - v_j}{x_i - x_j} \tag{2}$$

$$u_c = u_i - \theta_c (x_i - x_c) \tag{3}$$

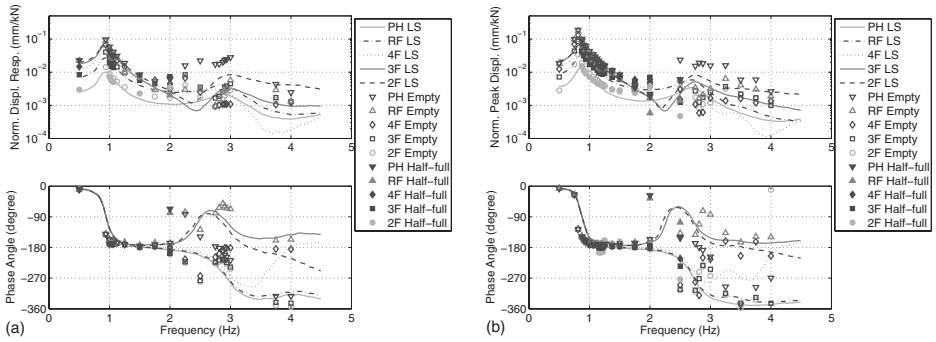


**Figure 9.** Amplitude and phase plot of normalized displacement curves by EMS test and transfer function from the linear shaker test. (a) N-S translational, and (b) and E-W translational.

$$v_c = v_i + \theta_c(y_i - y_c) \tag{4}$$

where $\theta_c$, $u_c$, and $v_c$ denote the story acceleration for rotation, N-S translation, and E-W translation of the reference point $(x_c, y_c)$, respectively. The subscripts $i$ and $j$ identify the two different sensors (accelerometers), respectively; thus, $(u_i, v_i)$ are measured acceleration from a sensor located at $(x_i, y_i)$. The reference point was selected as the mid-point between columns B2 and C2, approximately in the center of building plan (Figure 6). Since more than three channels of data were available for most floors, story accelerations from all combinations were computed and the average was taken as the final story acceleration. When all sensors at a given floor were working properly, story accelerations obtained from different sets of acceleration channels were almost identical, thereby validating the rigid diaphragm assumption. Strain and interstory displacement histories were measured during the LMS test; however, the signal-to-noise ratio was too low to obtain meaningful readings because of the low-level excitation. Transfer functions for LMS test data were evaluated as the ratio of the cross-spectral density function between input (shaker force) and output (story acceleration) to the auto-spectral density function of input, and are presented in Figure 9. The natural frequencies and the damping ratios from each dataset were obtained by linear system identification analyses and are presented in the sections that follow.

## ECCENTRIC MASS SHAKER TESTS

Essential data to characterize structural behavior at moderate-amplitude vibrations were generated by synchronizing the two EMS to provide excitation nominally in the N-S and E-W translational and torsional directions of the building. Tests in each direction were performed at two force amplitudes (i.e., empty and half-full baskets). E-W translation (Figure 1) and torsional excitation were induced by introducing a phase offset of 0° and 180° between the two shakers, respectively. Once the E-W translation and torsional tests were completed, the shaker configuration was modified to enable excitation in the N-S translational direction. The baskets were re-positioned such that the E-W

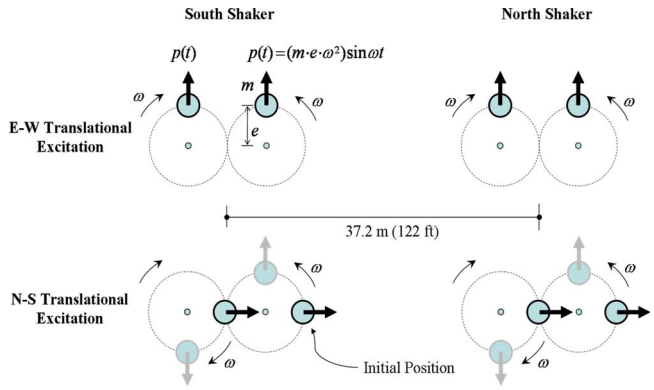


**Figure 10.** Initial positions of shaker baskets for E-W and N-S translational excitation.

component of the inertial force generated by one basket was cancelled by the E-W component of the other basket, producing a resultant force in the N-S direction (Figure 10).

Each of the tests began by ramping up the shaker rotation to the lowest target frequency of 0.5 Hz, and gradually increasing the target frequency until the limiting frequency (see Table 1) at which the maximum force capacity of the shakers was achieved. The target frequency was increased using increments of 0.0625 Hz, 0.125 Hz, and 0.25 Hz, with the smaller steps used around the natural frequencies identified using the ambient vibration data. The test duration at each target frequency was maintained for a minimum of 60 seconds to obtain steady state response. Example acceleration response histories are displayed in Figure 11. The steady-state motion clearly illustrates a re-

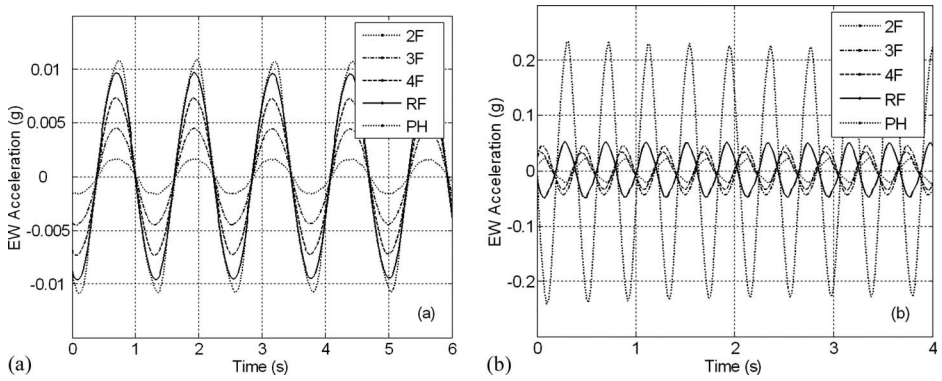


**Figure 11.** Acceleration response histories during E-W translational EMS testing with half-full baskets at forcing frequencies of (a) f=0.8125 Hz and (b) f=2.4375 Hz.

sponse dominated by first and second modes, respectively. Note the peak acceleration of 0.25 g was observed at the penthouse, whereas the primary lateral force resisting structure's peak response was an order of magnitude less.

Before proceeding to data interpretation, acceleration measurements at the ground floor were investigated to assess the importance of rocking motion of the building associated with foundation flexibility i.e., soil-structure interaction. Distributions of vertical acceleration revealed that rocking motion was not significant (Yu 2005), which is consistent with expectations for this relatively flexible moment frame building supported on caissons (Stewart et al. 1999). Thus, the effect of rocking motion was ignored in the analysis of test data.

Normalized displacement response curves were constructed using measured accelerations and the input force. The resulting input forcing function from the two synchronized shakers was estimated using the mass-eccentricity of baskets and the recorded pulse marker signals. The three components of story acceleration at the reference point of each floor were calculated from the measured accelerations using Equations 2–4. A narrow bandpass filter (a fifth-order Butterworth filter with cutoff frequencies of 50% and 150% of the excitation frequency) was applied for each frequency step to obtain a single frequency vibration signal. The peak amplitude of the story accelerations was determined from the steady state portion of the filtered signals. The peak amplitude was divided by the square of the circular frequency, and then normalized by the amplitude of the input forcing function to obtain the normalized displacement at each frequency. The phase lag of the normalized displacement with respect to the input force was obtained by subtracting 180° from the relative phase lag of the (bandpass filtered) story acceleration from the (bandpass filtered) input forcing function. Figure 9 shows the amplitude and phase spectra of the normalized displacement response curves obtained from the EMS tests for N-S and E-W translation and transfer function curves obtained from the LMS tests.

Figure 12 shows the typical variation of interstory drifts (during torsional EMS test with half-full baskets), calculated from the peak displacements and phase angles for each floor obtained from the story accelerations, at selected excitation frequencies. Because the floor displacements may be out of phase, except at resonance, the interstory drift is taken as the absolute value of the difference between two displacement vectors, normalized by the story height. Interstory drifts obtained from LVDT measurements were consistent with those obtained using this approach. However, due to dynamic interaction of the sensor mounts, LVDTs mounted with a spring support system, Figure 7e, the direct measurements were of poorer quality (e.g., clipping of data peaks occurred) than the acceleration data (Yu 2005). As shown in Figure 12, at frequencies less than about 2 Hz, interstory drifts are almost evenly distributed throughout the first to fourth stories; however, for higher frequencies, drifts at the roof and penthouse levels are substantially larger than those for lower stories. For all tests with the EMS, the maximum interstory displacement was 0.7 in. (0.43%) which was achieved at the north frame (Line 7 of Figure 1) between the fourth floor and roof under 2.4625 Hz torsional excitation with half-full baskets. It is important to note that, while substantial, this interstory

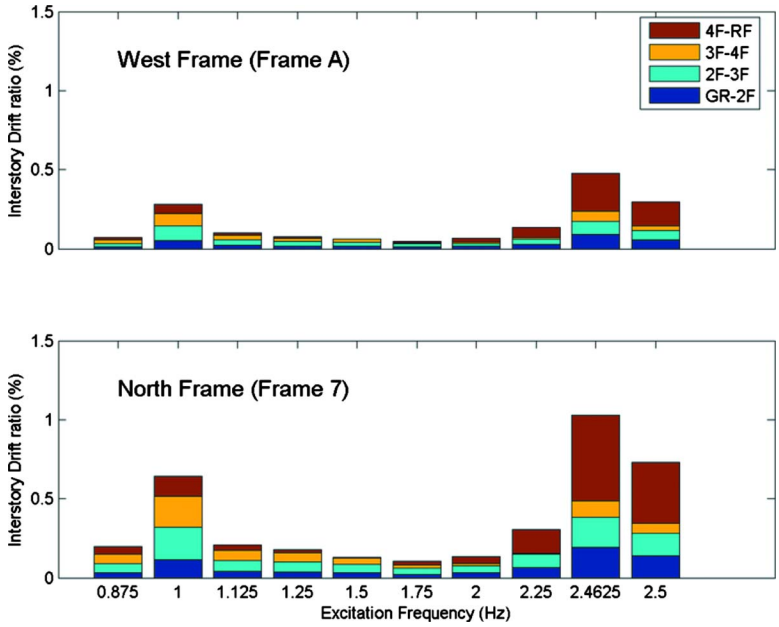


**Figure 12.** Interstory drift distribution during torsional EMS excitation with half-full baskets.

drift is insufficient to produce yielding given the relatively flexible moment frame system (e.g., see Wallace et al. 1998), as interstory drifts of roughly 1.0% to 1.5% are typically required to achieve yielding within moment frame systems.

Concrete strain gauges were attached to slabs and columns to monitor local deformations. Maximum compressive strain profiles for strain gauges attached to the fourth floor slab around Column B2 for N-S shaking with half-full basket tests are shown in Figure 13. In this figure, the area enclosed by measured strain distributions from the column centerline to the slab mid-span was determined from the measured strain data, and an effective (slab) width was calculated by dividing this area by the maximum strain (ACI 2002). The effective (slab) width estimated using this approach was approximately 0.4 $l_1$, where $l_1$ is the center-to-center span length in the direction of framing (30.5 ft). The FEMA-274 Commentary (BSSC 1997) includes the following equation for estimating the effective slab stiffness for reinforced concrete construction based on work by Hwang and Moehle (2000):

$$I_{\text{effective}} = \beta(2c_1 + l_1/6)t_{slab}^3/12 = \beta\alpha(l_1)t_{slab}^3/12 \quad (5)$$

where $c_1$ is the column dimension in the direction of framing (24 inches), $\beta$ is a factor used to represent the impact of cracking, $\alpha$ is commonly referred to as the effective slab width (without consideration of cracking), and $t_{slab}$ is the overall slab thickness. The effective slab width $\alpha$ for the building tested, obtained using Equation 5, is 0.43. For post-tensioned slabs $\beta$ values are typically between 2/3 and 1.0, resulting in $\alpha\beta$ values be-

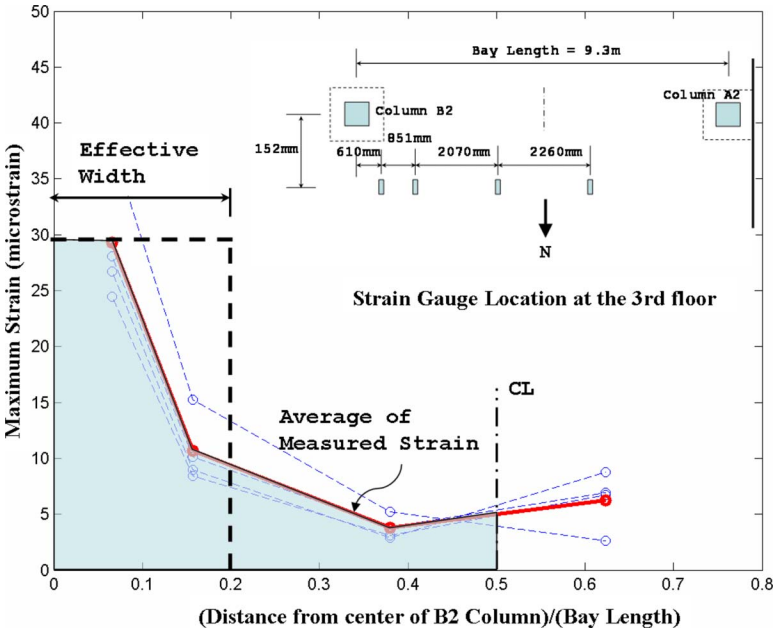


**Figure 13.** Maximum compressive strain distribution profile along the fourth floor slab at the B2 column during N-S translational excitation with half-full baskets.

tween 0.29 and 0.43. Kang and Wallace (2005) determined an effective width value of 0.47 ($\alpha$=0.7, $\beta$=2/3) using data obtained in shake table tests of an approximately 1/3-scale, two-story, post-tensioned flat plate by tuning the natural frequency of an analytical model to the results obtained from the tests. The cracked effective slab width of 0.4 obtained from Figure 13 is within the range of previously proposed and reported values, and would be a reasonable value to use in subsequent, detailed analytical studies of this building.

From the strain measurements obtained on three column faces at given locations, column curvature distributions were calculated. Although the calculated curvature distributions may be influenced by local cracking given the relatively small sensor gauge length, the computed curvature distributions are consistent with the preexisting damage survey. For example, in Figure 14a, the measured column curvatures at the second floor for Column B2 and the third floor for Column A2, where severe damage was observed (punching failure and joint diagonal cracks, respectively), are quite small relative to results obtained at apparently undamaged locations. Thus, at connections with no visible damage, moment transfer was observed indicating that the lack of visible damage was sufficient to determine the likelihood that full moment transfer capacity still existed after the Northridge earthquake. For visibly damaged connections, assuming the connection capacity to transfer shear and moment has dropped to a residual (post-punching) value, such as described in ASCE/SEI 41-06 Supplement #1 (Elwood et al. 2007), is reasonable.

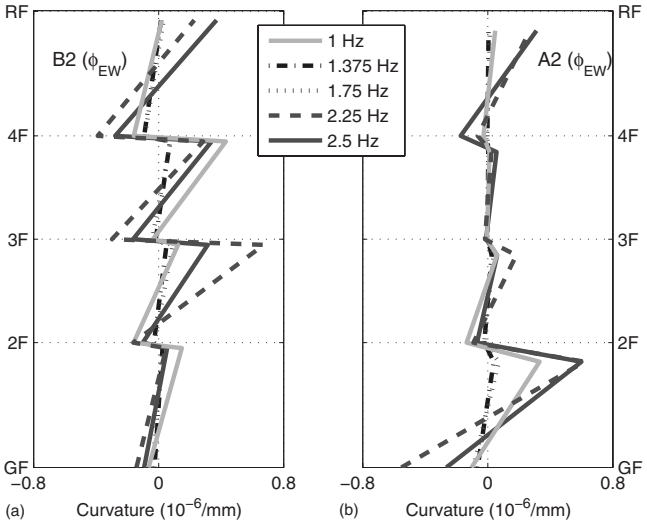


**Figure 14.** Curvature distributions along (a) B2 and (b) A2 column (E-W and torsional excitation with half-full basket 07/14, Curvature contributing to N-S directional deformation).

It is worth noting that field testing projects of this type present a number of unique challenges, such as equipment deployment (major equipment deployed on the roof with a crane), lack of power (various generators were used), and safety (broken glass, mold, poor lighting). Negotiating a lease agreement between the building owner and UCLA proved to be a challenge, despite a willing owner. However, the most formidable challenge was security, for both researchers and expensive equipment, given the length of the deployment (months). Since the building had been unoccupied for 10 years at the time of testing (due to damage from the Northridge earthquake in January 1994), it was a haven for transients who attempted to steal equipment (which had to be housed in secure rooms located on floors 2 through 4). A security firm was hired to observe the building after hours and researchers always worked in groups. Given these challenges, the research team typically worked long hours to minimize the length of the field deployment.

## SYSTEM IDENTIFICATION

Detailed investigation of modal properties was performed by system identification analyses. For the LMS and ambient vibration data, a linear time-domain system identification method available in the Matlab system identification toolbox, the Numerical Algorithm for Subspace State Space System Identification (N4SID) (van Overschee and DeMoor 1996), was adopted. It is noted that the damaged structure is expected to exhibit some nonlinear behavior over the *broad* range of responses, even for low-to-moderate level excitation amplitudes; however, it is common to use an effective (typically secant) flexural stiffness for responses up to the system yield strength (FEMA 356) to represent the amplitude dependent drop in effective stiffness. This approach is adopted, and verified by Yu et al. (2007a, 2007b). For the LMS test data, the input to system identification

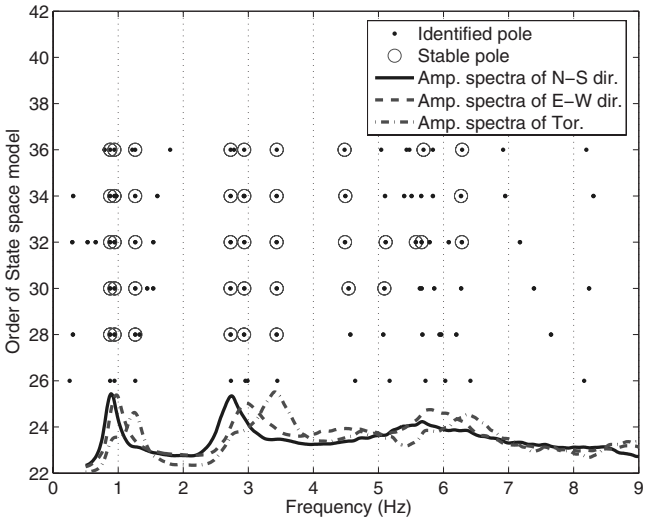


**Figure 15.** Stability plot.

analysis is the shaker force (obtained as the product of the measured acceleration of shaker table and the shaker mass), and the outputs are the three-story accelerations (two translations, one rotation) measured at the five floor levels, for a total of 15 outputs. The N4SID approach also was employed for ambient vibration measurements with the exception that input forcing function is not specified.

From the input and output, the N4SID estimates a state space model, via linear least squares, given the model order specified by the user. A state space model of order 30 should be sufficient to identify the 30 poles corresponding to the modal properties of the 15 modes. However, due to measurement noise and numerical round-off errors, not all of the identified modes from the system identification process have physical meaning. To distinguish the physical and non-physical (spurious) modes, a stability plot (Bodeux and Golinval 2001), which represents variations of identified natural frequencies, damping ratios, and mode shapes due to a change of model order, was employed. Figure 15 shows the stability plot for the LMS test run2, indicating all identified modes and their stability as the model order is increased from 28 to 36. In the figure, a robust mode is chosen as the mode satisfying the following stability conditions; the difference in results between the current and prior model should be: (1) less than 1.5% for natural frequency, (2) less than 5% for damping ratio, and (3) more than 98% for the Modal Assurance Criterion (MAC) (Allemang and Brown 1982). The first six or seven modes could be identified from each of the LMS test data and ambient vibration measurements. Despite the earthquake damage to the interior, slab-column connections, the cyclic response of the building frame is effectively linear given the low-to-moderate amplitude vibrations imposed during the tests (no element yield) and the light damage to the perimeter moment frame. That is, reloading, despite the modest damage resulting from the Northridge earthquake, is essentially linear with changes in observed frequencies expected due to concrete

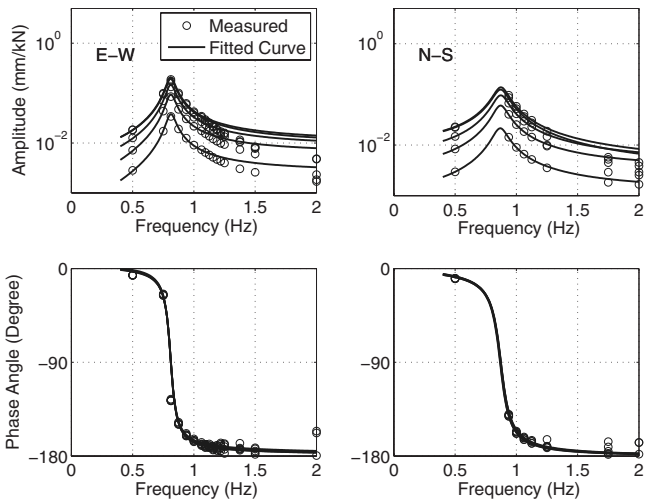


**Figure 16.** Curve-fitting of SDOF transfer function to EMS test data (empty basket).

cracking (drop in the effective flexural stiffness $E_cI_{eff}$). These assumptions were confirmed based on detailed model updating studies reported by Yu et al. (2007b, see Figure 11), where linear models using $E_cI_{eff}$ equal to a fraction of $E_cI_g$ for beams and columns were able to capture the measured displacement responses.

The natural frequencies in the E-W and N-S translational directions for the EMS tests were estimated by fitting analytical transfer function curves to the points on the normalized displacement response curve (Figure 16). The curve-fitting was performed only for fundamental frequencies using the transfer function of SDOF system using the points close to a −90° phase angle, since this approach is valid for a linear system. In general, the transfer function of a dynamic system can be expressed as

$$H(s) = \frac{N(s)}{D(s)} \tag{6}$$

where $s$ is a Laplace variable, $N(s)$ and $D(s)$ are matrix polynomials, respectively. For a SDOF system where the output is acceleration, $N(s)$ and $D(s)$ are second-order polynomials. Coefficients of second-order polynomials, $N(s)$ and $D(s)$, are evaluated for each degree of freedom using the Matlab function *invfreqs*. In the case of a MDOF system, the transfer function of the entire system is a linear combination of the transfer functions for each mode, each of which can be expressed as SDOF system. However, around a lightly damped fundamental frequency, the contributions from other (higher) modes are negligible, and the transfer function of the entire system is almost the same as that of the fundamental mode. Fundamental frequencies and damping ratios for each direction were taken as the average of the values determined from Equation 6 for each story. Curve fitting for the fundamental torsional mode was not as good as for the translation modes

**Table 3.** Identified natural frequencies

| Mode | E-W | N-S | Torsion | E-W | N-S | Torsion | Mixed |
|---|---|---|---|---|---|---|---|
| Identified Natural Frequency (Hz) | | | | | | | |
| Ambient 0702,(a) | 1.09 | 1.25 | 1.55 | 3.23 | 3.63 | 4.16 | 5.38 |
| EMS, (b) | 0.81 | 0.87 | 1.1～1.2 | — | — | — | — |
| Ambient 0719, (c) | 1.06 | 1.2 | 1.5 | 3.11 | 3.51 | 3.99 | — |
| LMS 0728, (d) | 0.87 | 0.94 | 1.25 | 2.73 | 2.91 | 3.43 | — |
| LMS 0802, (e) | 0.88 | 0.94 | 1.26 | 2.73 | 2.94 | 3.44 | 4.54 |
| Ambient 0803 (f) | 1.06 | 1.21 | 1.49 | 3.11 | 3.48 | 3.96 | — |
| Normalized to LMS 0802, (e) | | | | | | | |
| (a)/(e) | 1.24 | 1.33 | 1.23 | 1.18 | 1.24 | 1.21 | 1.19 |
| (b)/(e) | 0.92 | 0.93 | 0.87～0.95 | — | — | — | — |
| (c)/(e) | 1.20 | 1.28 | 1.19 | 1.14 | 1.19 | 1.16 | — |
| (d)/(e) | 0.99 | 1.00 | 1.00 | 1.00 | 0.99 | 1.00 | — |
| (f)/(e) | 1.20 | 1.29 | 1.19 | 1.14 | 1.18 | 1.15 | — |
| Normalized to the fundamental frequency for each direction | | | | | | | |
| Ambient 0702 | 1.00 | 1.00 | 1.00 | 2.96 | 2.90 | 2.68 | — |
| EMS | 1.00 | 1.00 | 1.00 | — | — | — | — |
| Ambient 0719 | 1.00 | 1.00 | 1.00 | 2.93 | 2.93 | 2.66 | — |
| LMS 0728 | 1.00 | 1.00 | 1.00 | 3.14 | 3.10 | 2.74 | — |
| LMS 0802 | 1.00 | 1.00 | 1.00 | 3.10 | 3.13 | 2.73 | — |
| Ambient 0803 | 1.00 | 1.00 | 1.00 | 2.93 | 2.88 | 2.66 | — |

due to coupling between modes; however, the natural frequency for the fundamental torsional mode was determined to be around 1.1 to 1.2 Hz.

Identified natural frequencies are presented in Table 3. The frequencies identified with the EMS data and ambient vibrations data were, on average, 8% lower and 14% to 35% higher than those obtained using the LMS test data, respectively. Since there was no change in building mass during the tests, these differences are attributed to changes in stiffness properties due to either the contribution of nonstructural elements and/or amplitude dependent stiffness degradation of structural members due to concrete cracking. However, for this building, the contribution of non-structural elements was thought to be relatively minor since most of the drywall partitions were already separated from neighboring structural members due to earthquake damage and no in-filled or exterior brick veneer walls exist. Consequently, amplitude dependent stiffness degradation due to concrete cracking is the more likely cause of the frequency drop.

Previous researchers have observed the dependence of the natural frequencies on the amplitude of vibration. Foutch (1978) reported that the fundamental frequencies decreased from 5% to 7% based on a 15-fold increase in the excitation force. Trifunac (1972) also found that the natural frequencies obtained by forced vibration test were about 4% lower that those obtained using ambient vibration data. Well documented sub-

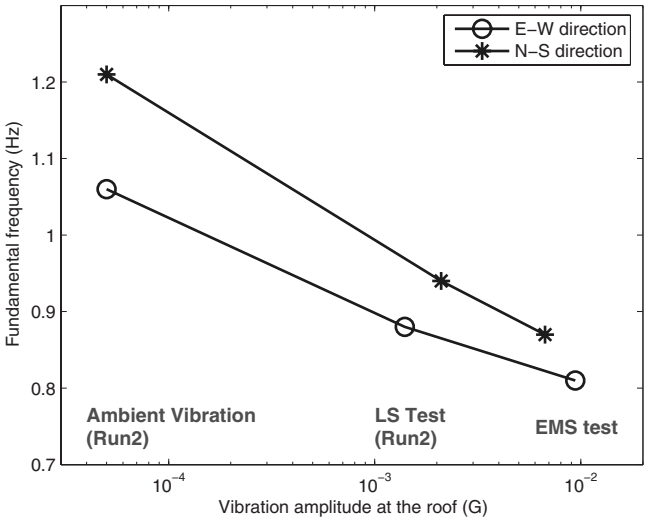


**Figure 17.** Change of natural frequencies with vibration amplitude.

sequent studies further validate the earlier findings, e.g., Celebi et al. (1993). In the current tests, the peak values of the roof accelerations around the fundamental frequencies, obtained by filtering data with a very narrow bandpass filter (fifth-order Butterworth filter with cutoff frequencies of 95% and 105% of the fundamental frequencies in each test), are $5 \times 10^{-5}$ g, 0.0015 g to 0.002 g, and 0.007 g to 0.009 g for the ambient, LMS tests, and EMS tests, respectively. The relationship between shaking amplitude and fundamental frequency is shown in Figure 17. The decrease in fundamental frequencies appears to be proportional to the logarithm of the (filtered) vibration amplitude increase.

Table 3 also shows the ratios of identified natural frequencies to the lowest fundamental frequency for each direction. Frequency ratios for the forced vibration and ambient vibration tests follow different trends, that is, the first N-S frequency is 7% to 8% higher than the first E-W frequency for the forced-vibration tests (EMS test and LMS tests), and 13% to 14% higher for the ambient vibration tests. The changes in the frequencies indicate that stiffness degradation occurs for larger amplitude vibrations, and is more severe in the structural members contributing to stiffness in the N-S direction. As noted earlier, this is attributed to a drop in the effective flexural stiffness ($E_c I_{eff}$) due to concrete cracking. It is noted that the larger stiffness drops in the NS direction were attributed primarily to joint cracking (Yu et al. 2007b; see Figure 3b).

As shown in row (a) and (f) of Table 3, identified frequencies for ambient vibration measurements collected after the half-full basket EMS test showed a 3% to 4% reduction in frequencies relatively to the ambient vibration results identified prior to the test. Amplitude dependent shaking stiffness reduction (i.e., due to concrete cracking) in structural members, exterior cladding, or foundation/soil supporting the building may be responsible for this result.

**Table 4.** Identified damping ratios

| Mode | E-W | N-S | Torsion | E-W | N-S | Torsion | Mixed |
|---|---|---|---|---|---|---|---|
| Ambient 0702 | 2.93% | 4.87% | 1.78% | 1.86% | 3.18% | 2.29% | 3.68% |
| EMS | 4.4% | 6.6% | — | — | — | — | — |
| Ambient 0719 | 3.35% | 3.10% | 2.14% | 2.98% | 3.07% | 2.14% | — |
| LMS 0728 | 5.90% | 6.88% | 6.17% | 5.84% | 8.24% | 6.19% | — |
| LMS 0802 | 5.66% | 6.94% | 6.01% | 5.61% | 7.69% | 6.14% | 13.50% |
| Ambient 0803 | 2.92% | 2.98% | 1.31% | 2.24% | 2.98% | 2.60% | — |

The ratios of the identified frequencies for the second modes to identified frequency for the first modes in each direction are in the range of 2.7 to 3.1 (Table 3). A ratio of 3.0 is commonly expected value for shear (frame) buildings (Trifunac 1972); therefore, the identified frequencies are consistent with expected results. Damping ratios identified from LMS tests and ambient vibrations are shown in Table 4, and mode shapes determined using LMS test data (run2) and ambient vibration data (run2) are shown in Figure 18. The first six mode shapes correspond to the (E-W) translation (Modes 1 and 4), (N-S) translation (modes 2 and 5), and torsion (modes 3 and 6). However, for the seventh mode identified, N-S translation and torsion appear to be mixed. The mode shapes are not as sensitive to the test method (i.e. vibration amplitude) as are the natural frequencies. Damping ratios for the LMS and EMS (Table 4) are within the range (5%) typically used for low-to-moderate level responses for reinforced concrete buildings (CTBUH 2006).

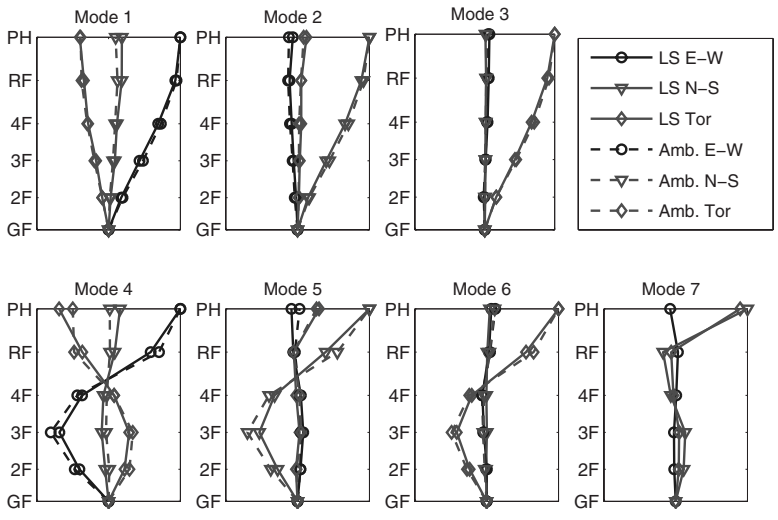


**Figure 18.** Mode shapes (Linear Shaker test Run2 and Ambient vibration Run2).

## CONCLUSIONS

A series of forced and ambient vibration tests were performed on a four-story reinforced concrete building damaged by the Northridge earthquake using the *nees*@UCLA mobile field laboratory. Two EMS and a LMS were used as vibration sources. Global frequency response of the test building and detailed behavior of structural components were monitored with a dense instrumentation array.

Acceleration measurements obtained during the tests were used to verify the rigid diaphragm assumption and also assess the quality of the data collected from direct interstory displacement measurements. The findings from the LVDT data indicate that dynamic interaction between the sensor mounts and the building produced clipping of peak values. The LVDT results still proved useful in verifying and interpreting the interstory displacements obtained using accelerometer data. The results indicate that care must be exercised in design of the instrument mounts, although use of a non-contact sensor would have obvious advantages.

From the strain measurements obtained during EMS test, the effective slab width was obtained as $0.41_1$, which is reasonably consistent with values obtained for other post-tensioned slab systems. Column curvature readings indicated that moment transfer capacity was lower at connections with visible damage relative to connections without visible damage. Therefore, detailed nonlinear modeling studies of the damaged building could be based on the visual damage survey, i.e., the unbalanced moment transfer strength for connections with visible damage could be assumed to have dropped to a residual value as described in FEMA 356 (ASCE 2000) or ASCE/SEI 41-06 (ASCE 2006).

From the acceleration measurements, variations in the modal properties of the building were investigated using system identification techniques. The first six to seven frequencies, damping ratios, and mode shapes for the building could be identified using the test results. Fundamental frequencies determined from the EMS test were only 70% to 75% of those determined using data collected during the ambient vibration tests, and 92% to 93% of those determined using the LMS test data. The cause of these shifts in natural frequencies is likely due to the influence of concrete cracking and the effect of preexisting cracks, including cracking observed in the joints.

The use of the dense instrumentation enabled a number of significant questions to be answered. For example, the assumptions that the diaphragm could be assumed to be rigid and that "soil-structure-foundation-interaction" was insignificant could be verified. Further, the use of strain gauges enabled the determination of an effective slab width and to relate observed damage (or lack of) at slab-column connections to ability of the connection to transfer moments during the test (after the earthquake). Redundancy of data measurements also increased the robustness of these results. Future studies will involve assessing reasons and the degree of building damage that resulted from the Northridge earthquake. The information derived from this study will assist in the development of the baseline linear response of the undamaged building, which will then be subjected to site specific ground motions to predict the degree and severity of nonlinear responses.

## ACKNOWLEDGMENTS

The authors gratefully acknowledge that this research was conducted with equipment purchased and integrated into the *nees*@UCLA Equipment Site with support from NSF Cooperative Agreement CMS-0086596. Additional support was provided by the National Science Foundation (Award Number CMS-0301778) to conduct the testing and analytical studies reported. The authors gratefully acknowledge the assistance of undergraduate interns supported by the Pacific Earthquake Engineering (PEER) Center (NSF Award EEC-9701568), Xiao Xuan (Sam) Du and Andrew Parker, and the Center for Embedded Networked Sensing (CENS) (NSF Cooperative Agreement CCR-0120778), Michael Contreras, Genevieve Farrar, Sarah Taylor-Lange. The assistance provided by *nees*@UCLA System Administrator Steve Kang, *nees*@UCLA Senior Development Engineer Mr. Steve Keowen, and NEES System Integration team member Mr. Paul Hubbard was greatly appreciated. Finally, the authors would like to thank the building owner, M. David Paul, and Mr. Don Dodd of Krismar Construction for their cooperation which enabled this research.

## REFERENCES

Abdel-Ghaffar, A. M., and Scott, R., 1980. Dynamic properties of earth dams, *Proceedings, 7th World Conference on Earthquake Engineering*, pp. 371–378, Istanbul, Turkey.

Allemang, R. J., and Brown, D. L., 1982. A correlation coefficient for modal vector analysis, *Proceedings, 1st International Modal Analysis Conference*, Orlando, Florida, pp. 110–116.

American Concrete Institute (ACI) Committee 318, 2002. *Building Code Requirements for Structural Concrete and Commentary (ACI 318–02)*, ACI, Farmington Hills, Michigan.

American Society of Civil Engineers (ASCE), 2000. *Prestandard and Commentary for the Seismic Rehabilitation of Buildings (FEMA 356)*, Reston, VA.

——, 2006. *Seismic Rehabilitation of Existing Buildings: Supplement #1 (ASCE/SEI 41-06)*, Reston, VA.

Aschheim, M., and Moehle, J. P., 1995. *Four-story flat-slab building in Sherman Oaks*, *Preliminary Build. Case Study Rep. to ATC-33*, Berkeley, California.

Bodeux, J. B., and Golinval, J. C., 2001. Application of ARMAV models to the identification and damage detection of mechanical and civil engineering structures, *Smart Mater. Struct.* **10**, 479–489.

Bolt, B. A., and Hudson, D. E., 1975. Seismic instrumentation of dams, *J. Geotech. Eng. Div.* **101**, 105–1104.

Building Seismic Safety Council (BSSC), 1997. *NEHRP Commentary on the Guidelines for the Seismic Rehabilitation of Buildings (FEMA Publication 274)*, ATC-33 Project, Washington, D.C.

California Strong Motion Instrumentation Program (CSMIP) 2006. California Geological Survey, Department of Conservation, http://www.conservation.ca.gov.cgs/smip/about.htm.

Celebi, M., Phan, L. T., and Marshall, R. D., 1993. Dynamic characteristics of five buildings during strong- and low-amplitude motions, *International Journal of the Structural Design of Tall Buildings* **2**, 1–15.

Council on Tall Buildings and Urban Habitat (CTBUH), 2006. White Paper—CTBUH Seismic Working Group, http://www.ctbuh.org/.

Doebling, S. W., Farrar, C. R., Prime, M., and Shevitz, D. W., 1996. *Damage identification and health monitoring of structural and mechanical systems from changes in their vibration characteristics: A literature review*. Los Alamos National Laboratory LA-13070-MS.

Dye, T. M., and Halling, M. W., 2002. Forced vibration testing of a permanently instrumented full-scale bridge, *Proceedings, 7th U.S. National Conference on Earthquake Engineering*, Paper 163, 10 pp., Boston MA.

Elwood, K. J., Matamoros, A. B., Wallace, J. W., Lehman, D. E., Heintz, J. A., Mitchell, A. D., Moore, M. A., Valley, M. T., Lowes, L. N., Comartin, C. D., and Moehle, J. P., 2007. Update to ASCE/SEI 41 Concrete Provisions, *Earthquake Spectra* **23**, 493–523.

Foutch, D. A., 1978. The vibrational characteristics of a twelve-storey steel frame building, *Earthquake Eng. Struct. Dyn.* **6**, 265–294.

Foutch, D. A., and Jennings, P. C., 1978. A study of the apparent change in the foundation response of a nine-story reinforced concrete building, *Bull. Seismol. Soc. Am.* **68**, 219–229.

Galambos, T. V., and Mayes, R. C., 1979. Lessons form dynamic tests of an eleven storey building, *Eng. Struct.* **1**, 264–273.

Imamura, A., Hijikata, K., Tomii, Y., Nakai, S., and Hasegawa, M., 1996. An experimental study on nonlinear pile-soil interactioni based on forced vibration tests of a single pile and a pile group, *Proceedings, 11th World Conference on Earthquake Engineering*, Paper 563, Acapulco, Mexico.

Hudson, D. E., 1960. A comparison of theoretical and experimental determination of building responses to earthquakes, *Proceedings, 2nd World Conference on Earthquake Engineering*, Japan, pp. 1105—1119.

——, 1961. *A new vibration exciter for dynamic tests of full scale structures*, Earthquake Engineering Research Laboratory, California Institute of Technology, 19 [20].

——, 1962. *Synchronized vibration generators for dynamic tests of full-scale structures*, Earthquake Engineering Research Laboratory, California Institute of Technology, 33 [43].

——, 1977. Dynamic tests of full-scale structures, *J. Engrg. Mech. Div.* **103**, 1141–1157.

Hueste, M. D., and Wight, J. K., 1997. Evaluation of a four-story reinforced concrete building damaged during the Northridge earthquake, *Earthquake Spectra* **13**, 387–414.

Hwang, S.-J., and Moehle, J. P., 2000. Models for laterally load slab-column frames, *ACI Struct. J.* **97**, 345–353.

Ibáñez, P., Chien, S., Dinyavari, M., Dobbs, M., Gundy, W., Howard, G., Keowen, R., Rentz, P., Smith, C., Stoessel, J., Walton, W., and Sires-Yifat, C., 1981. Methods and benefits of experimental structural dynamic evaluation of nuclear power plants, *Nucl. Eng. Des.* **64**, 1–32.

International Conference of Building Officials (ICBO), 1976. *Uniform Building Code*, ICBO, Whittier, California.

Jennings, P. C., Matthiesen, R. B., and Hoerner, J. B., 1972. Forced vibration of a tall steel-frame building, *Earthquake Eng. Struct. Dyn.* **1**, 107–132.

Kang, T. H.-K., and Wallace, J., 2005. Dynamics responses of flat plate systems with shear reinforcement, *ACI Struct. J.* **102**, 763–773.

MathWorks, Inc., 2004. *MATLAB*, Natick, MA.

Muto, K., and Kobayashi, T., 1973. Simulation analysis on a reinforced concrete building model, *Transactions of the Architectural Institute of Japan* **205**, 43–51.

Nastase, D., 2005. Dynamic Behavior of Nonstructural Elements and Systems during Full Scale Building Vibration Experiments, M.S. thesis, University of California, Irvine, 281 pp.

National Instruments, *Labview 7 User Manual*, April 2003.

Paek, J., Kothari, N., Chintalapudi, K., Rangwala, S., Xu, N., Caffrey, J., Govindan, R., Masri, S., Wallace, J., and Whang, D., 2005. The performance of a wireless sensor network for structural health monitoring, *2nd European Workshop on Wireless Sensor Networks*, Istanbul, Turkey.

Petrovski, J., Paskalov, T., and Jurukovski, D., 1974. Dynamic full-scale test of an earthfill dam, *Geotechnique* **24**, 193–206.

Sabol, T. A., 1994. Flat slab failure in ductile concrete frame building, *1994 Northridge Earthquake Buildings Case Studies Project*, Proposition 122: Product 3.2, SSC 94-06, Seismic Safety Commission, State of California, Sacramento, California.

Skolnik, D., Lei, Y., Yu, E., and Wallace, J. W., 2006. Identification, model updating, and response prediction of a 15-story steel frame building, *Earthquake Spectra* **22**, 781–802.

Stephen, R. M., and Bouwkamp, J. G., 1977. Dynamic behavior of an eleven story masonry building, *Proceedings, 6th World Conference on Earthquake Engineering*, Meerut, India, pp. 2711–2716.

Stewart, J. P., Seed, R. B., and Fenves, G. L., 1999. Seismic soil-structure interaction in buildings. II: Empirical findings, *J. Geotech. Geoenviron. Eng.* **125**, 38–48.

Trifunac, M. D., 1972. Comparisons between ambient and forced vibration experiments, *Earthquake Eng. Struct. Dyn.* **1**, 133–150.

van Overschee, P., and DeMoor, B., 1996. *Subspace Identification of Linear Systems: Theory, Implementation, Applications*, Kluwer Academic Publishers.

Wallace, J. W., McConnell, S. W., Gupta, P., and Cote, P. A., 1998. Use of headed reinforcement in beam-column joints subjected to earthquake loads, *ACI Struct. J.* **95**, 590–606.

Whang, D. H., Kang, S. W., Wallace, J. W., Stewart, J. P., Yu, E., and Lei, Y., 2004. Integration of NEESgrid into the *nees*@UCLA field testing site, *13th World Conference on Earthquake Engineering*, Vancouver, B.C., Canada, Paper No. 0486.

Yu, E., 2005. Forced Vibration Testing and Analytical Modeling of a Four-Story Reinforced Concrete Frame Building, Ph.D. thesis, University of California, Los Angeles.

Yu, E., Taciroglu, E., and Wallace, J. W., 2007a. Parameter identification of framed structures using an improved finite element model updating method—part I: formulation & validation, *Earthquake Eng. Struct. Dyn.* **36**, 619–639.

Yu, E., Wallace, J. W., and Taciroglu, E., 2007b. Parameter identification of framed structures using an improved finite element model updating method—part II: applications to experimental data, *Earthquake Eng. Struct. Dyn.* **36**, 641–660.

(Received 4 January 2006; accepted 7 July 2008)